Original

Li, D.; Storch, H.v.; Yin, B.; Xu, Z.; Qi, J.; Wei, W.; Guo, D.:

Low−Level Jets Over the Bohai Sea and Yellow Sea: Climatology, Variability, and the Relationship with Regional Atmospheric Circulations

In: Journal of Geophysical Research : Atmospheres (2018) AGU

DOI: 10.1029/2017JD027949

Journal of Geophysical Research: Atmospheres

RESEARCH ARTICLE
10.1029/2017JD027949

Key Points:
- The model robustly reproduces the climatology, daily cycle features, variability of wind profiles, and specific low-level jet cases
- Low-level jets feature strong interannual, intra-annual, and diurnal cycle variability but weak decadal variability
- There is a strong link between the low-frequency anomaly of low-level jet occurrence and regional atmospheric circulations

Supporting Information:
- Supporting Information S1

Correspondence to:
Z. Xu,
xuzhenhua@qdio.ac.cn

Citation:
Li, D., von Storch, H., Yin, B., Xu, Z., Qi, J., Wei, W., & Guo, D. (2018). Low-level jets over the Bohai Sea and Yellow Sea: Climatology, variability, and the relationship with regional atmospheric circulations. *Journal of Geophysical Research: Atmospheres*, *123*, 5240–5260. https://doi.org/10.1029/2017JD027949

Received 25 OCT 2017
Accepted 5 MAY 2018
Accepted article online 15 MAY 2018
Published online 31 MAY 2018

Low-Level Jets Over the Bohai Sea and Yellow Sea: Climatology, Variability, and the Relationship With Regional Atmospheric Circulations

Delei Li[1,2], Hans von Storch[3,4,5], Baoshu Yin[1,2,6], Zhenhua Xu[1,2], Jifeng Qi[1,2], Wei Wei[7], and Donglin Guo[8]

[1]Key Laboratory of Ocean Circulation and Waves, Institute of Oceanology, Chinese Academy of Sciences, Qingdao, China, [2]Function Laboratory for Ocean Dynamics and Climate, Qingdao National Laboratory for Marine Science and Technology, Qingdao, China, [3]Institute of Coastal Research, Helmholtz Zentrum Geesthacht, Geesthacht, Germany, [4]CliSAP, University of Hamburg, Hamburg, Germany, [5]College of Oceanic and Atmospheric Sciences, Ocean University of China, Qingdao, China, [6]University of Chinese Academy of Sciences, Beijing, China, [7]State Key Laboratory of Severe Weather, Chinese Academy of Meteorological Sciences, Beijing, China, [8]North China Sea Marine Forecasting Center of State Oceanic Administration, Qingdao, China

Abstract The present study reveals climate features of low-level jets (LLJs) over the Bohai Sea and Yellow Sea (BYS) based on a 35-year (1979–2013) high-resolution (7 km) atmospheric hindcast. The regional climate model COSMO-CLM driven by the ERA-Interim reanalysis data set was used to obtain the hindcast. Through comparison with observations, the hindcast was proved to robustly reproduce the climatology, the diurnal cycle, the variability of wind profiles, and specific LLJ cases. LLJs over the BYS feature a strong diurnal cycle, intra-annual, and interannual variability but weak decadal variability. LLJs are more frequent in April, May, and June (LLJ season) and less frequent in winter over the Bohai Sea and western coastal areas of the Yellow Sea, which is due to the intra-annual variations of large-scale circulation and local land-sea thermal contrast. In the LLJ season, the heights of jet cores are generally lower than 500 m above sea level. The maximum wind speed of LLJs is mostly in the range of 10–16 m/s, and prevailing wind directions are southerly and southwesterly. The LLJs are of the nocturnal type, with the highest occurrence frequency at approximately 2300 local time. Furthermore, a low-frequency link between anomalies of LLJ occurrence and regional large-scale barotropic circulation was identified using canonical correlation analysis and associated correlation patterns. Pressure systems over the East Asia-northwest Pacific region are significantly correlated with the variations of LLJ occurrence over the BYS in terms of the intra-annual and interannual variability.

1. Introduction

Low-level jets (LLJs) are mesoscale-flow phenomena with horizontal wind maxima within the lowest few kilometers of the troposphere (e.g., Stensrud, 1996). They are strongly linked to the deep convective activity and mesoscale convective complexes (Maddox, 1983; Means, 1954). LLJs affect transport and mixing processes in the atmospheric boundary layer by modifying the vertical wind shear and the turbulence structure, thus conditioning the formation of convective fog, clouds, and heavy rainfall events (Chen et al., 2005; Muñoz & Enfield, 2011; Nuss et al., 2000).

Over water regions, ocean dynamics, and the air-sea coupling processes are impacted by LLJs (Beardsley et al., 1987). The coastal-parallel winds of offshore LLJs enhance the upwelling of deeper and cold waters near coasts, which results in decreases of sea surface temperature and ocean surface evaporation. This contributes to the aridity and dryness of some coastal regions such as the Peruvian coastal desert strip (Nicholson, 2010; Warner, 2004). LLJs are also significant for human activities, such as aviation safety, offshore wind energy applications, sound propagation, fishery resources, and the transport of pollutants (Arfeuille et al., 2015; Nunalee & Basu, 2013).

There have been extensive studies on LLJs over regions worldwide including, but not limited to, North America (Higgins et al., 1997), Europe (Soares et al., 2017), South America (Marengo et al., 2004), and Asia (Du et al., 2014). Over the land, the most renowned LLJs that have been intensively studied are the Great Plains LLJs over North America (Blackadar, 1957; Higgins et al., 1997; Parish & Oolman, 2010), which are most

frequent during the warm seasons from April to October and are greatly influenced by the sloping terrain of the Rocky Mountains. They are highly ageostrophic, with wind speed maxima reached shortly after midnight.

Over water regions, typical LLJs are those found along coastal regions (Doyle & Warner, 1993). Coastal LLJs are frequently linked with large-scale atmospheric circulation, land-sea thermal contrast, and coastal terrain (Parish, 2000). They are synoptically driven but mesoscale intensified: the high-pressure system over the land and low-pressure inland are the synoptic forces of coastal-parallel flows. The local wind intensification occurs due to the sharp thermal and associated pressure gradients, with strong baroclinic structures (Burk & Thompson, 1996). Furthermore, the interaction with topography may enhance coastal LLJ winds or cause them to change in direction, when high mountain ranges exist along the coast (Chao, 1985; Jiang et al., 2010). Coastal LLJs generally feature a diurnal cycle, with wind speed maximum at midafternoon (Ranjha et al., 2013). The wind maxima are generally at low altitudes and are constrained by the marine atmospheric boundary layer capping the temperature inversion (Rijo et al., 2018).

Ranjha et al. (2013) constructed a global distribution map of coastal LLJs based on ERA-Interim reanalysis for summer and winter seasons and found that they are essentially a summer phenomenon. Except for those along the southeast Arabian Peninsula (Ranjha et al., 2015) and New York Bight Jet (Colle & Novak, 2010), coastal LLJs are mainly distributed along the eastern boundary current regions, including the west coasts of North America, South America, the Iberian Peninsula, and northwestern and southern Africa. Coastal LLJs over these regions have been extensively studied based on field observations (Rahn & Parish, 2007; Winant et al., 1988) and/or on model and theoretical efforts (Burk & Thompson, 1996; Cardoso et al., 2016; Rijo et al., 2018; Soares et al., 2014, 2017). However, not all LLJs in the coastal regions are the typical coastal LLJs, as defined by Ranjha et al. (2013). Over the Caribbean region, the wind speed exhibits a distinct jet-like profile, while the temperature shows a decreasing profile vertically. The strong meridional surface temperature gradients are thought to force Caribbean LLJs (Cook & Vizy, 2010), although this was still under debate until recently (Maldonado et al., 2017).

Over the Chinese coastal areas, Wei et al. (2014) investigated the features and evolutions of LLJs at two sites (Tianjin and Shanghai) along the northern coast of China using wind profile radar data sets in summer. They found that nocturnal LLJs overwhelmed daytime LLJs in both strength and frequency, and distinct LLJ wind directions and heights were observed due to the different local topography and synoptic forcing at the two sites. Based on high-resolution (9 km) model data, Du et al. (2015) found strong LLJs off the southeastern coast of China, with jet cores at the 925-hPa level. The generation was subject to a large-scale setting enhanced by land-sea thermal contrast and coastal orographic effects. Unlike typical coastal LLJs, LLJs off the southeastern coast of China feature nocturnal wind maximum instead of midafternoon wind maximum, and the LLJ wind maxima do not reside within the sloping temperature inversion layer.

Thus, while many studies on the physics or climate of LLJs worldwide have been performed, limited studies (Du et al., 2015) have examined the mechanisms behind the formation and life cycle of LLJs in Chinese coastal areas. Studies on the climatology, including the variability on diurnal and intra-annual and interannual time scales, and on decadal trends have rarely been performed for these LLJs. With our study, we present a climatology and variability of LLJs over the Bohai Sea and Yellow Sea (BYS) regions, spatially and temporally. Furthermore, the relationship of LLJs with regional large-scale forcing in low-frequency was also studied. A 35-year-long high-resolution (7 km) simulation of the regional climate model COSMO-CLM (CCLM, Rockel et al., 2008) was used.

The present study is organized as follows: section 2 describes the used data sets, including the forcing data set, observations, and CCLM data set, as well as the identification criteria of LLJs. Section 3 discusses the model evaluation using the sounding data and wind profile data from different stations. Section 4 presents the climatology and annual cycle variability of LLJs, as well as the diagnosed mechanisms for monthly variations of the LLJs. In section 5, we describe the variability and large-scale conditioning during LLJ season. A summary and conclusions are given in the final section 6.

2. Data and Methodology

2.1. Regional Climate Model Simulation

The nonhydrostatic regional atmospheric model CCLM version 4.14 was used to construct the atmospheric conditions over the BYS (see Figure 1) from 1979 to 2013. The model was developed from the Local Model

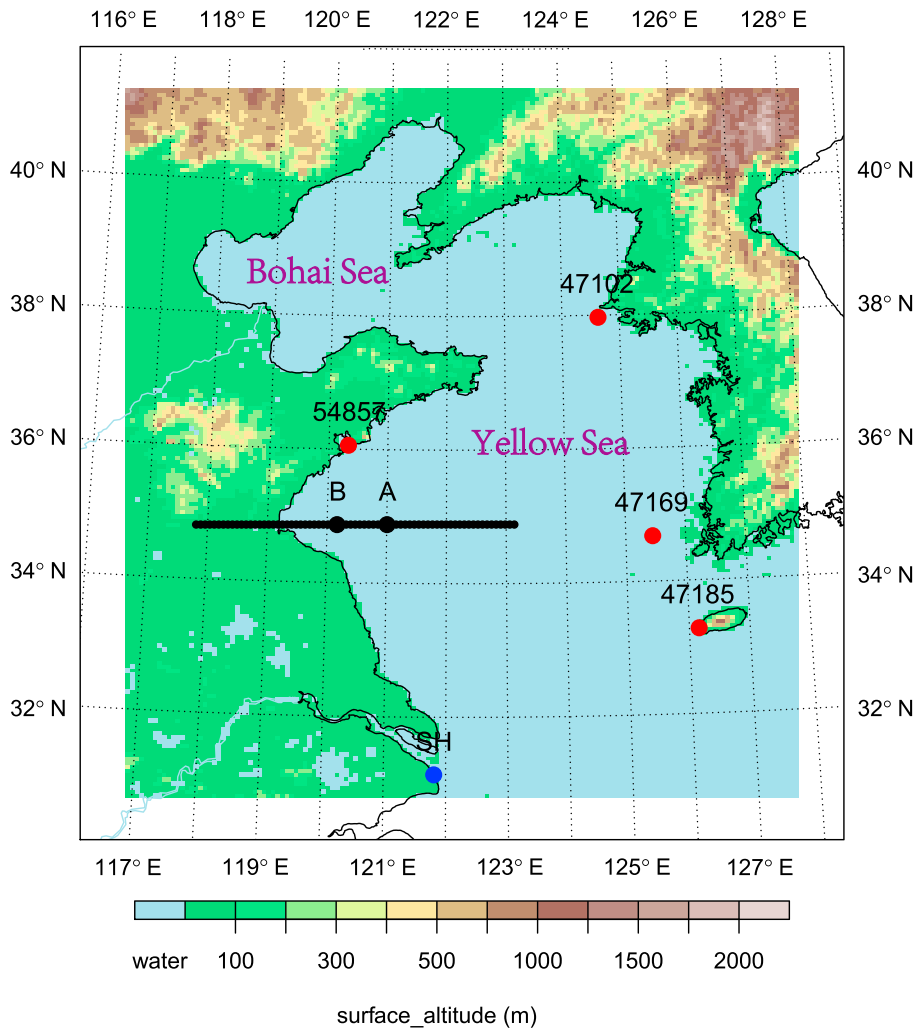

Figure 1. Orography of the simulation domain. Red points indicate four radiosonde observations (47102: 124.63°E, 37.97°N; 47169: 125.45°E, 34.68°N; 47185:126.16°E, 33.28°N; 54857: 120.33°E, 36.06°N); blue point (121.81°E, 31.14°N) represents location of wind profiler radar observation. The black line marks the cross section, point A (121.00°E, 34.88°N) and point B (120.12°E, 34.87°N) are for low-level jet cases study. The white frame indicates the sponge zone.

of the Deutscher Wetterdienst (German Weather Service) and is now widely used in mesoscale climate studies with spatial grid resolutions in the range of 1–50 km.

The constraining conditions for CCLM used in the study were obtained from the global atmospheric reanalysis ERA-Interim (ERAI, Dee et al., 2011). ERAI is produced by the European Centre for Medium-Range Weather Forecasts. It is available from 1 January 1979 to the present and is supposed to continue until the end of 2018. The horizontal resolution of ERAI is approximately 80 km (T255 spectral), and the temporal output interval is 6 hr. It has shown better quality in producing low-frequency variability and stratospheric circulation than its predecessor ERA-40 (Dee & National Center for Atmospheric Research Staff, 2018).

CCLM adopts a rotated geographical coordinate with an Arakawa C-grid structure. A generalized terrain-following height coordinate system was used to keep the lowest surface of the constant vertical coordinate conformal to the orography. The horizontal resolution of our simulation was 0.0625° (~7 km). Ranjha et al. (2016) evaluated the impact of varying resolutions (from 54 to 2 km) on the model's ability to resolve features of a coastal LLJ over California coasts and concluded that 6 km is a compromise resolution that reproduces most of the features of a coastal jet. Together with another study (Du et al., 2015), this indicates that such a 7-km grid resolution is reasonable for simulating the features of LLJs over the BYS.

Ten grid boxes were set as the sponge zone in the lateral boundary at each side. Forty layers were used in the vertical direction, with higher resolution in the lower troposphere. The temporal output interval for winds in vertical levels was 3 hr. When identifying LLJs, we used wind data at the lowest 18 levels, that is, 10, 34.5, 69, 116, 178.5, 258.5, 357.5, 477, 618.5, 782.5, 970, 1,182.5, 1,420, 1,682.5, 1,927.5, 2,290, 2,635, and 3,007.5 m.

The simulation time step was 60 s. An interior spectral nudging technique (von Storch et al., 2000) was used in the simulation every third time step on the horizontal U and V wind components with levels above 850 hPa. This aimed to keep the simulated large-scale pattern consistent with that of ERAI and to develop the local and regional physical processes on their own. The Tiedtke convective parameterization scheme (Tiedtke, 1989) was used for cumulus convection. The multilayer soil and vegetation model TERRA-ML scheme (Schrodin & Heise, 2002) was used for land surface processes. A prognostic TKE-based scheme (Mellor & Yamada, 1982) was used for vertical turbulent transport.

2.2. Observations

Due to the unavailability of wind observations at upper-air levels in the BYS, four radiosonde observations in the near coastal area (red points in Figure 1; 47102 [1 January 2001 to 31 December 2013], 47169 [1 January 2004 to 31 December 2013], 47185 [1 January 1997 to 31 December 2013], and 54857 [1 January 1997 to 31 December 2013]) were obtained from the atmospheric soundings data set archive of the University of Wyoming (http://weather.uwyo.edu/upperair/sounding.html) to validate the model data set. The radiosonde observations are available twice daily, at 0000 and 1200 UTC. Multiple variables, such as temperature, wind speed, wind direction, and dew point temperature, at different pressure levels (and corresponding height levels) are included in the data sets. Furthermore, more observation data were obtained from a boundary layer wind profile radar, which was operated in the Yangtze River Delta of China (blue point in Figure 1). The data are of high frequency and high vertical resolution (50 m); they have been used to study the features and evolution of LLJs along the Chinese coast (Wei et al., 2013). The quality of CCLM in representing the diurnal cycle and specific LLJ cases will be assessed based on wind profile radar observations.

2.3. Identification Criteria of LLJs

Previous studies identified LLJs based on various criteria (Bonner, 1968; Ranjha et al., 2013; Tao & Chen, 1987). Some researchers identified LLJs using the horizontal wind maxima at the 1,000-, 925-, 850-, or 700-hPa levels without requiring a vertical shear threshold of the horizontal winds (Tao & Chen, 1987; Wang et al., 2013; Whyte et al., 2007). Ranjha et al. (2013) developed an algorithm to identify the typical coastal LLJ globally based on the vertical profiles of wind speed and temperature, requiring that the wind speed maximum within a temperature inversion of the marine atmospheric boundary layer. This algorithm has been used widely in climatological studies of regional coastal LLJs (Ranjha et al., 2015; Rijo et al., 2018; Semedo et al., 2016; Soares et al., 2014). However, this method will rule out LLJs at the top of the temperature inversion layer (which has been improved by Lima et al., 2018) and may rule out those are not locally generated but remotely propagating.

In the present study, we adopted the criteria defined by Bonner (1968), in which the thresholds of three parameters are defined as certain values, including the maximum wind speeds, height of maximum winds, and magnitude of vertical shear above the jets. This basic detection method defines the LLJs by examining the horizontal wind maximum vertically, without considering the associated generation mechanism. These criteria were widely used or adopted in later literature (Doubler et al., 2015; Du et al., 2014; Miao et al., 2018; Pham et al., 2008; Wei et al., 2014; Whiteman et al., 1997; Wu & Raman, 1998). The threshold values vary due to the strength, distribution, and background circulation of LLJs.

The following thresholds were used to identify a LLJ in a vertical column: (1) the maximum wind speed is greater than 10 m/s in the lowest 18 layers (below ~3 km); (2) the difference between the wind maximum and minimum above or the wind speed at ~3 km is greater than 5 m/s; and (3) the wind maximum does not occur at the surface (the lowest model level at 10 m). The algorithm was applied to vertical profiles of wind speeds at all model grids over the BYS every 3 hr from 1979 to 2013. When a LLJ was identified, the jet location, jet height, jet speed, and direction were recorded. LLJ height is the height of the horizontal wind speed maximum, and LLJ direction refers to the wind direction at the LLJ height.

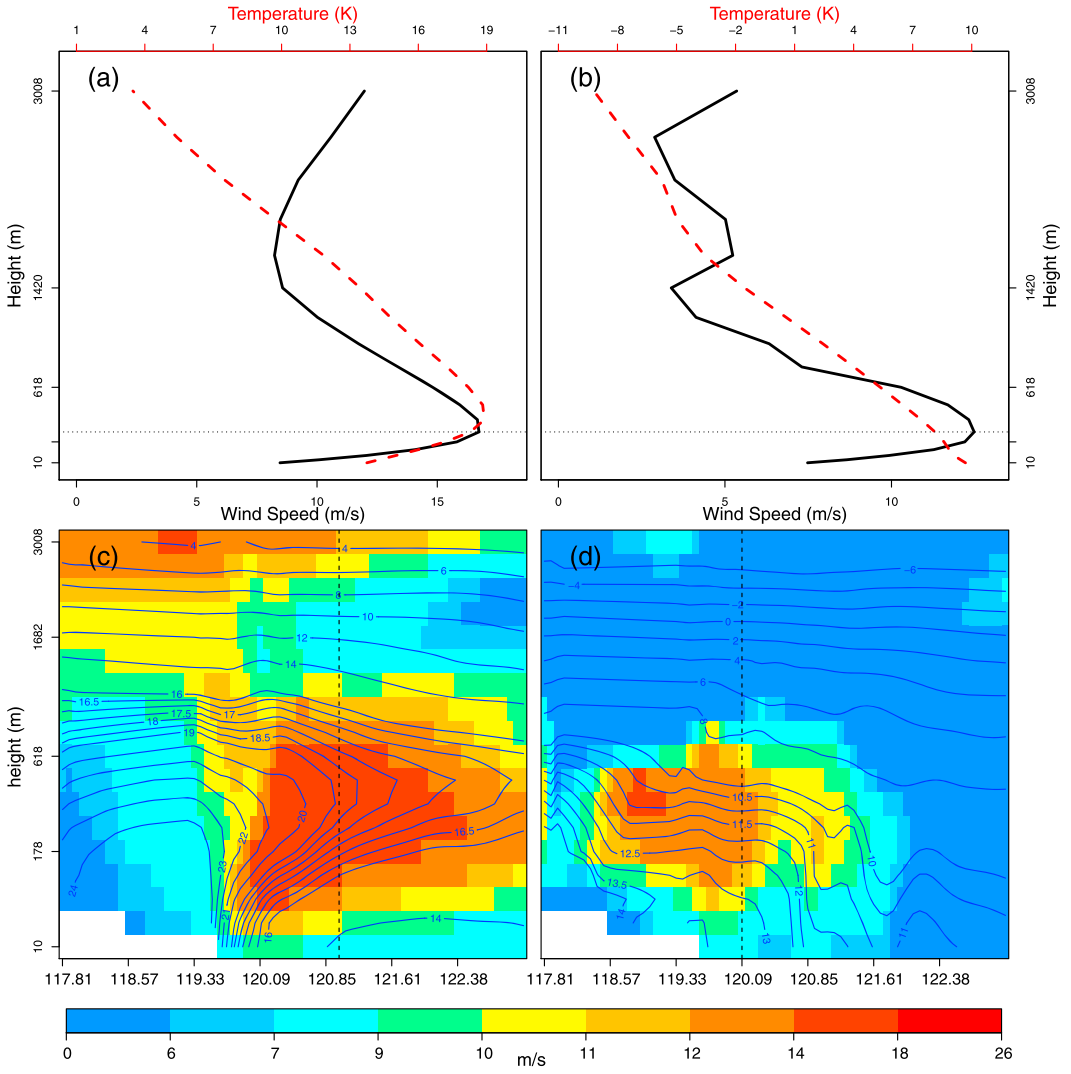

Figure 2. The vertical profiles of wind speed and temperature for (a) point A, (b) point B, and (c and d) the black cross section in Figure 1 at 14:00 LST on 3 April 2006 (left panel) and at 20:00 LST on 17 April 2007 (right panel), respectively. The horizontal dot lines in (a) and (b) are heights of wind maxima, black lines for wind speeds, and red lines for temperature. The dashed line in (c) and (d) are profile locations of point A and point B, respectively; contours are for temperature.

Figure 2 shows the vertical profiles of two LLJ cases detected using the algorithm. The wind speed maxima are approximately 15 m/s at low levels for both cases; however, case 1 (Figure 2c) features a sloping temperature inversion layer, with a maximum horizontal temperature gradient. The wind speed maximum resides within the sloping layer (Figures 2a and 2c), and it resembles the structure of typical coastal LLJ such as Oman coastal jets (Ranjha et al., 2015). Regarding case 2, the wind speed exhibits a distinct jet-like profile, since the temperature is decreasing with the height (Figure 2b). We can also observe a strong land-sea thermal contrast near the coasts, while there is no pronounced temperature inversion layer associated with this LLJ case (Figure 2d).

3. Evaluation of the Model Data Set

The model output has been applied to investigate present surface wind climate and added value to the description of winds by downscaling over the BYS (Li, 2017; Li, Geyer, & Bisling, 2016; Li, von Storch, & Geyer, 2016a, 2016b). Simulated surface winds have been assessed by comparing against satellite and in situ observation data both on land and over water. The results revealed that CCLM reliably represents the regional wind characteristics over the BYS area, with more detail than the driving ERAI reanalysis in the complex

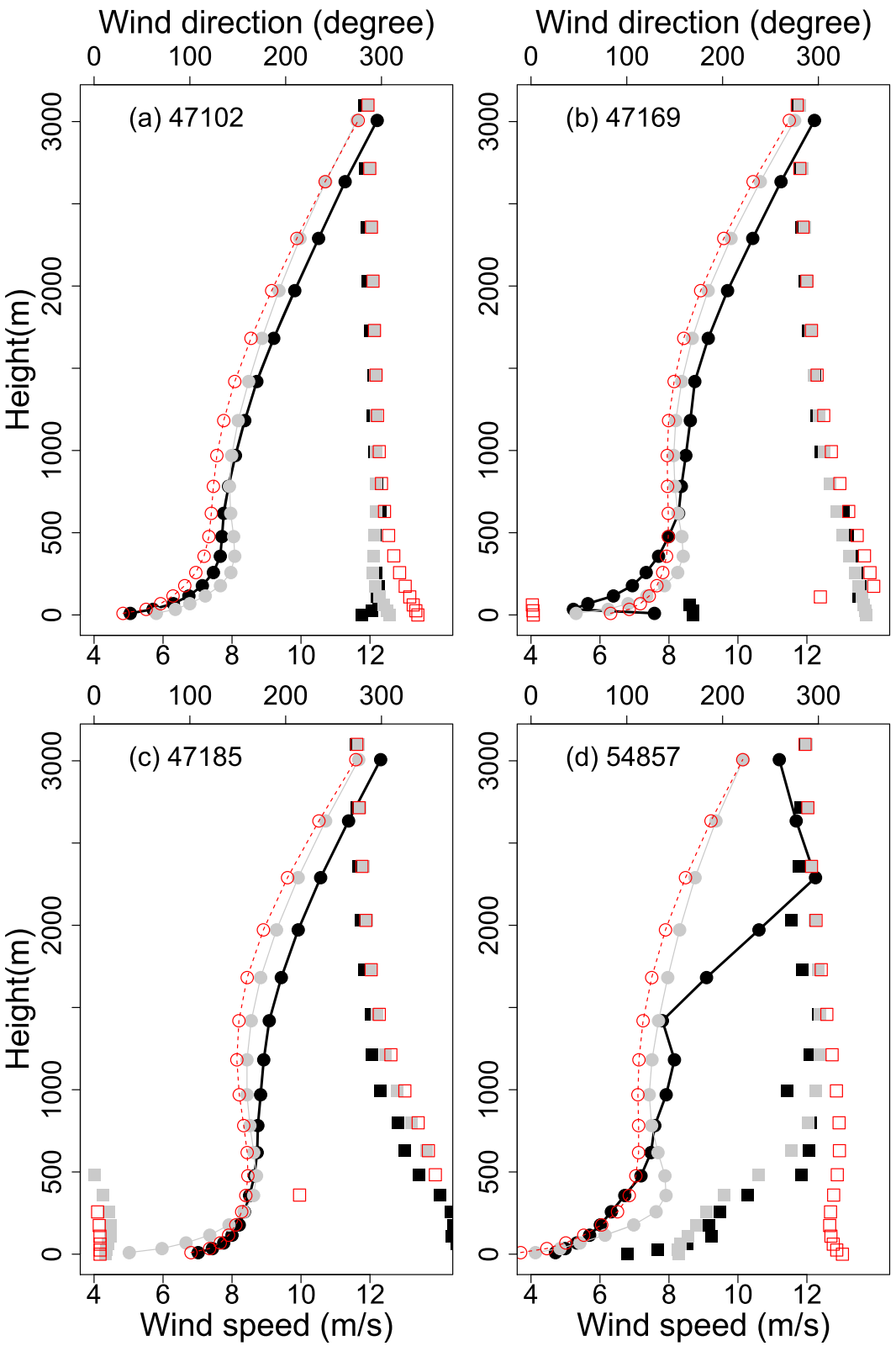

Figure 3. Climatological mean of vertical wind speed and wind direction of observation data (black dot line for wind speed and black squares for wind direction), CCLM data (gray dot line for wind speed and gray squares for wind direction) and ERA-Interim data (red dashed line for wind speed and red squares for wind direction).

Table 1
The First Two EOFs for Radiosonde Observations (OBS) and Simulation Data (CCLM) at Pressures Levels of 925, 850, and 500 hPa at Station 47102 From 2005 to 2008

	925 hPa		850 hPa		500 hPa		Var_percentage (%)	
EOFs	OBS	CCLM	OBS	CCLM	OBS	CCLM	OBS	CCLM
EOF1	0.26	0.27	0.29	0.31	0.92	0.91	73.6	72.7
EOF2	0.68	0.70	0.62	0.59	−0.39	−0.41	22.4	24.1

Note. EOFs = empirical orthogonal functions; CCLM = climate model COSMO-CLM.

coastal areas—in terms of wind intensities and directions, the wind probability distribution and extreme winds at mountain areas (Li, 2017). With respect to mesoscale atmospheric processes, CCLM outperforms ERAI in resolving detailed temporal and spatial structures for the phenomena of a typhoon, a coastal atmospheric front, and a vortex street. The data set has also been applied to the study of the climatology, variability, and extremes of wind energy over the BYS (Li, Geyer, & Bisling, 2016). In the following, we sought to assess how about the quality of CCLM in reproducing vertical profiles of the wind.

Four radiosonde observations (red points in Figure 1) were used to validate the reliability of CCLM in reproducing the climatology of wind profiles and its added value to ERAI. We interpolated CCLM and ERAI grid data to the radiosonde observation locations using the nearest-neighbor method and obtained temporal averaged for wind profiles. Figure 3 shows that the simulated climatology of the vertical profiles of wind speeds is generally in agreement with that of the observation data, except at station 54857, where the simulated wind speeds largely underestimated the observations at levels above 1,500 m. At station 54857, the observed wind generally shifts from southeasterly to northwesterly from the bottom level to the upper level below 3,000 m, whereas at the other stations, the wind directions are generally around 300°, which was reproduced by the CCLM data set. Additionally, although CCLM does not add value to the description by ERAI in capturing wind intensities, it outperforms ERAI in capturing observed wind direction at levels below 1,000 m. The observed strong wind at a high level for station 54857 may have been due to a wind intensification caused by the local topography or some local-scale phenomena, which were not resolved by either the coarse-resolution ERAI analysis or the CCLM analysis.

In addition to climatological features, the annual cycle was compared, showing generally consistent wind patterns and intensities between the CCLM data set and radiosonde observations at the different levels of 925, 850, and 500 hPa at the four stations (not shown here). Furthermore, based on the empirical orthogonal function (EOF) analysis method, the temporal evolution of the dominant patterns of wind speed (after subtraction of the annual cycle) has been compared between two data sets. The first two EOF modes and

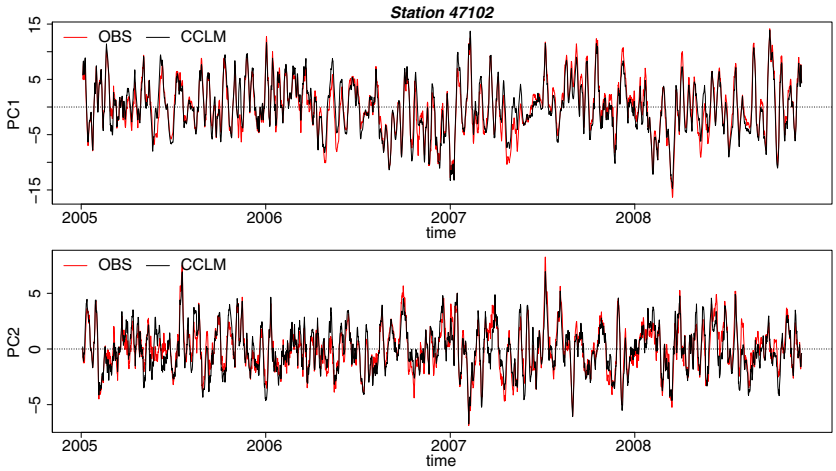

Figure 4. Time series of the principal coefficients of the first two empirical orthogonal function modes for radiosonde observations (OBS, red line) and simulation data (CCLM, black line) at pressures levels of 925, 850, and 500 hPa, with annual cycle subtracted at station 47102 in the period 2005–2008.

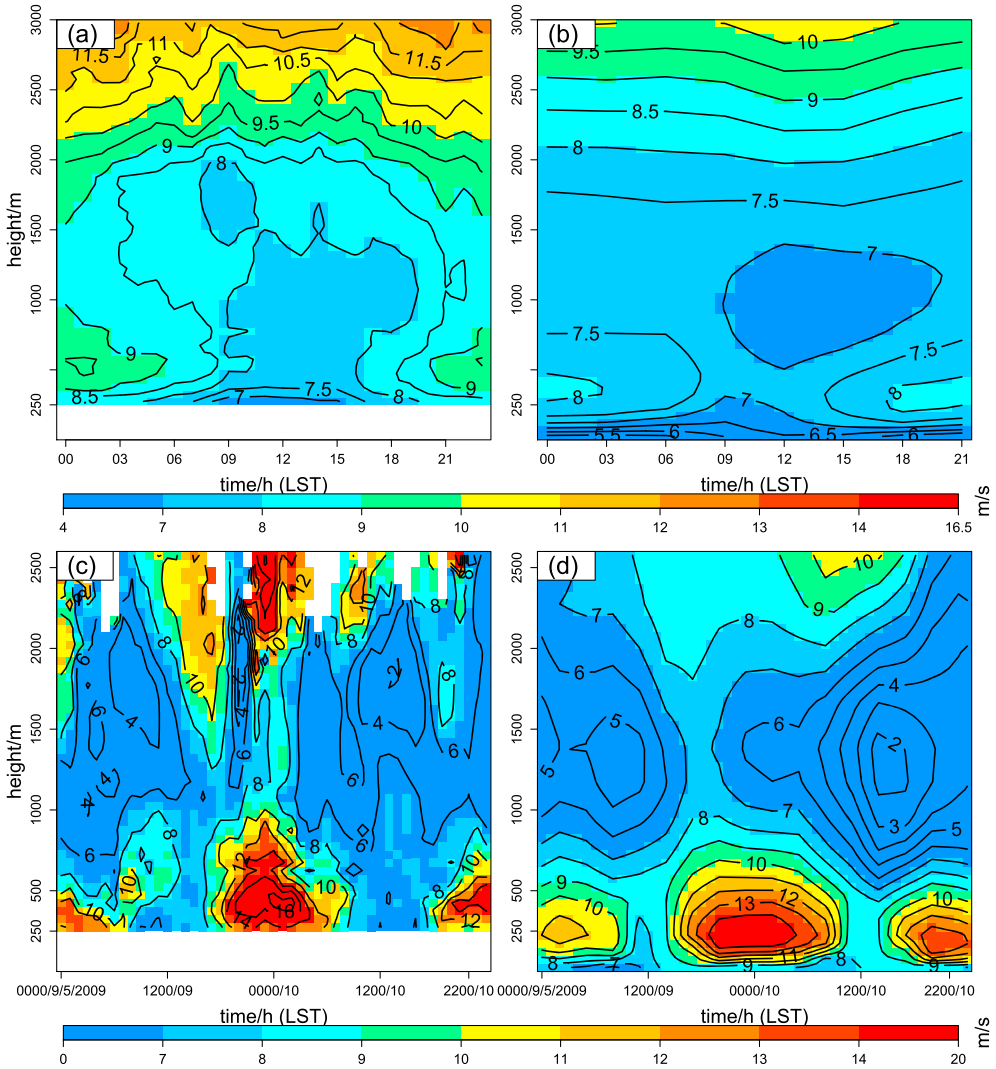

Figure 5. (a) Observed and (b) modeled daily height-time cross section of mean wind speeds during 2009; (c) observed and (d) modeled low-level jet cases: Height-time cross section of wind speeds during 0000 LST on 9 May 2009 to 0000 LST on 11 May 2009 at station SH (blue point in Figure 1). (a) and (c) were reproduced from Wei et al. (2013).

corresponding time series of principal coefficients, using station 47102 as an example, are given in Table 1 and Figure 4, respectively. The first EOF mode (Table 1) is dominant and explains almost 73% of the total variance; it shows that wind speed anomalies fluctuated in phase but that their intensities increased with height. The total variance explained by the second EOF mode is more than 22%, and this mode is out of phase between low (925 and 850 hPa) and upper (500 hPa) levels. All EOF patterns and temporal evolution of modeled wind speeds at different levels are consistent with those observed, which was also revealed by the results at the other three stations (data not shown), verifying the robustness of the CCLM wind data set.

Furthermore, the simulated daily climatology of wind profilers and LLJ cases at station SH (blue point in Figure 1) was compared with wind profiler radar observations for the year 2009 (Figure 5). For observations, the wind speeds are more uniform during the day than at night because of the stronger turbulent mixing in the boundary layer during the day (Figure 5a). From the late afternoon to early morning the next day, there is a layer with larger wind speeds in the range of 300–700 m. Above 2,000 m, strong wind speeds greater than 9 m/s are persistent in the daily cycle, and the wind speed increases with height. The spatial-temporal structure of our simulated wind profile (Figure 5b) is consistent with the observations, with underestimations of 1–2 m/s in wind speed intensities. Strong temporal variability (data not shown) lasts for the entire diurnal cycle and generally increases from 2 m/s in the surface to more than 8 m/s above 5,000 m. The patterns are

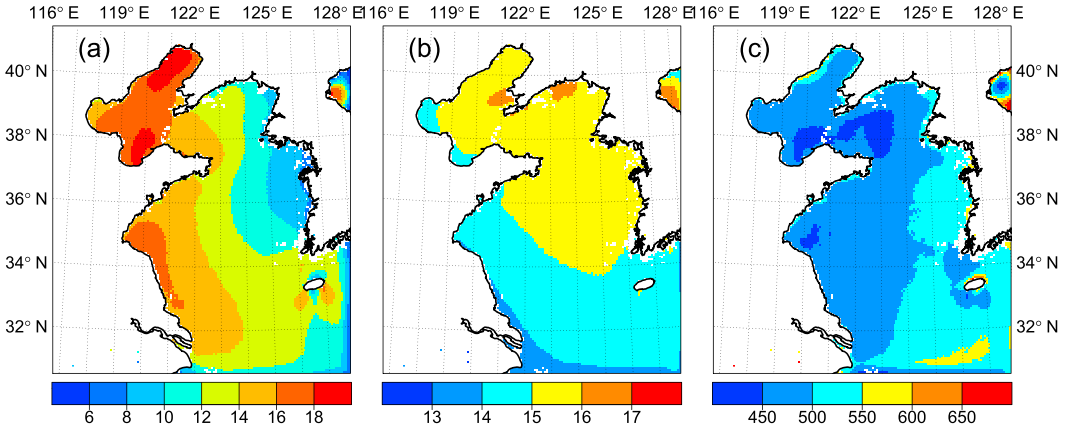

Figure 6. (a) Annual mean frequency of occurrence (%) of low-level jet (LLJ), (b) LLJ mean wind speed (m/s), and (c) LLJ mean occurrence height (m).

also consistent between the modeled and observed results, with some underestimation in strength by our model.

A modeled LLJ process (Figure 5d) from 2300 local solar time (LST) on 8 May 2009 to 0000 LST on 11 May 2009 shows a typical jet that occurred at a height of 100 to 700 m in the late afternoon and persisted until the next early morning, which is generally consistent with the diurnal cycle climatology in Figures 5a and 5b. The strength of the LLJ from 2000 LST on 9 May to 0500 LST on 10 May 2009 is stronger than that of its predecessor and successor. The simulated onset and developing features of LLJ are generally consistent with the observations (Figure 5c), while the simulated wind intensities of the LLJ underestimate the observations. Details of the wind structure patterns in the upper 2,000 m could not be well resolved by CCLM, which may be due to the coarse temporal resolution or some physical processes unresolved by the CCLM model.

In summary, based on the radiosonde observations and wind profiler radar observations, our model is robust in reproducing the climatology of wind profiles, the diurnal cycle, and the variability of wind speeds as well as LLJ cases.

4. Climatology and Annual Cycle of LLJs

As shown in section 2.3, the identification criteria were applied to the high-resolution hindcast data set from 1979 to 2013. The statistical analyses in the following sections are based on the identified LLJ information data set over the BYS region.

4.1. Intra-Annual Climatology and Variability

The annual mean frequency of LLJ occurrence (Figure 6a) is in the range of 8%–20% over the BYS, being more frequent over the Bohai Sea (BS) and western coastal areas of the Yellow Sea (YS; >14%) than over the coastal areas of the Korean Peninsula. The mean wind speeds of LLJs (Figure 6b) are stronger over the BS and the north YS (>15 m/s) than those in the south YS and two bays of the BS (13–15 m/s). The LLJ mean heights are generally lower than 500 m in the BS and northern and northwestern YS and are mostly in the range of 500–600 m in the southeastern part of our study domain, except for in the areas around Jeju Island.

Figure 7 shows a strong intra-annual variability of LLJ occurrence over the BYS. In winter, the LLJ occurrence is very low, with values mostly <12% from December to February. In contrast, the frequency is generally greater than 21% in April, May, and June; it is even greater than 30% in April and May over the BS and part of the western YS. March, July, and August are transition periods, when it is mostly in the range of 9–24%.

The spatial patterns of LLJ generation from March to August are similar but with different intensities, and larger values are distributed in the western part of the BYS and lower values in the eastern part of the BYS. The spatial patterns of the other months are different. From September to February, LLJs are more frequent over the BS and south or southeast of the YS than over the north and middle YS. The spatial distributions of monthly mean wind speeds of LLJs (see Figure S1 in the supporting information) show that the intensities

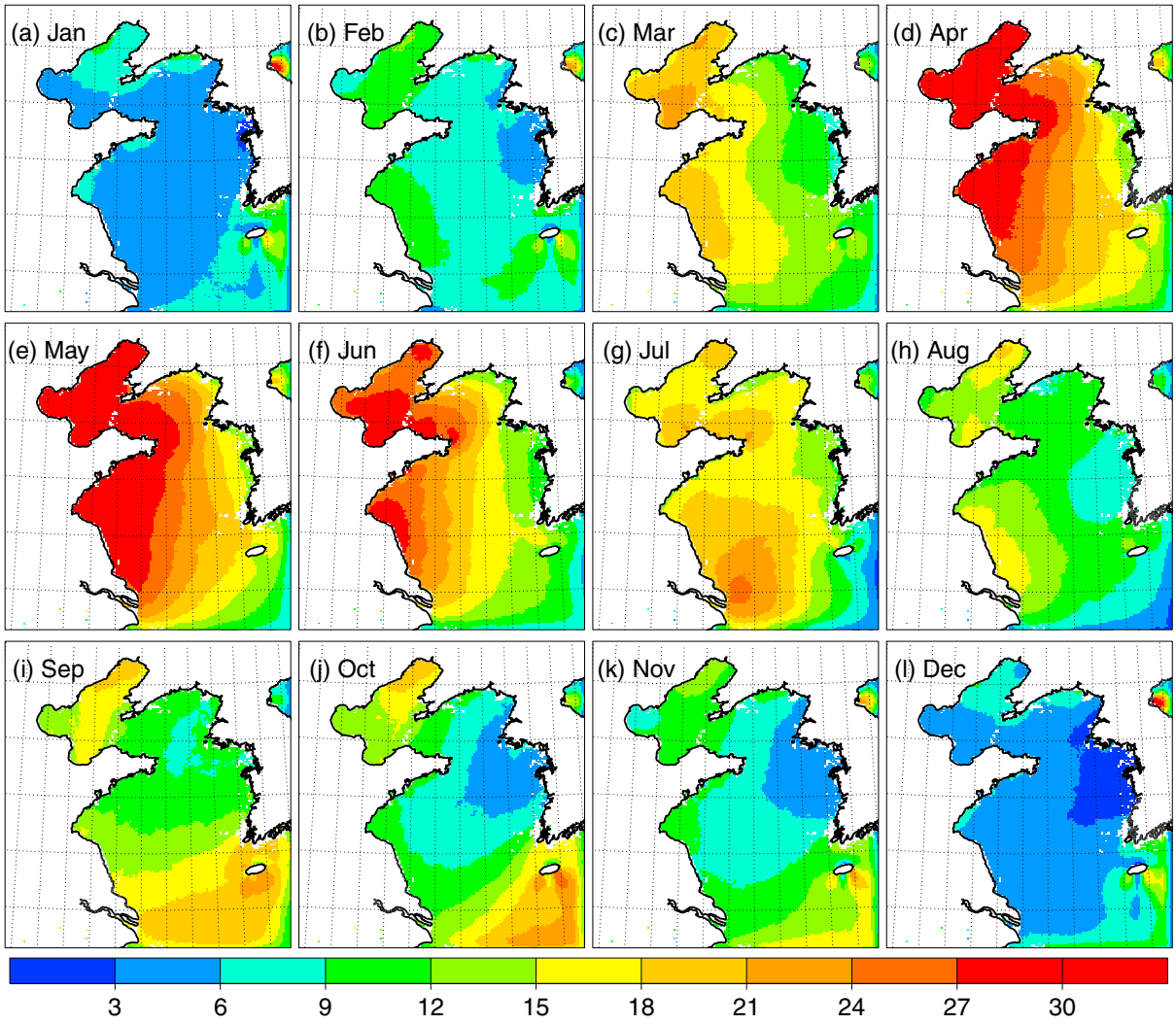

Figure 7. Spatial distributions of monthly occurrence frequency (%) of low-level jet.

over the BS are stronger from November to May (>16 m/s) and weaker in the other months, especially in July and August (<14 m/s). For the YS areas, we observe stronger LLJs from February to May, mainly in the north or middle YS areas (>16 m/s). Weaker LLJs from June to January are mainly distributed over the west YS coasts or the south YS areas (<14 m/s). In terms of the monthly mean height of LLJs (see Figure S2), they are mostly in the range of 450–700 m from August to December and mostly within 400–550 m from January to March. The LLJs are higher in the south YS than the north YS or the BS. The LLJ cores are generally located in the range of 400–650 m from April to June, with larger values in the south and southeast YS and west coasts of the Korean Peninsula (>500 m). LLJ cores in July are the lowest among all the months, with values mostly lower than 500 m.

However, the spatial distributions of monthly relative standard deviation (i.e., the standard deviation divided by the mean, in percentage) of LLJ occurrence (Figure 8) show different patterns from the monthly occurrence frequency of LLJs (Figure 7). They reveal that the relative interannual variability of monthly generation is generally greater than 20% in most areas and features strong variability within different months. From March to July, the relative standard deviations are mostly less than 50%, with values increasing from the northwest to southeast. In the other months, there is strong interannual variability especially in January and December, when the relative standard deviation reaches >90%. Therefore, strong interannual variability exists for LLJs over the BYS, especially during months when the LLJ occurrence is less frequent.

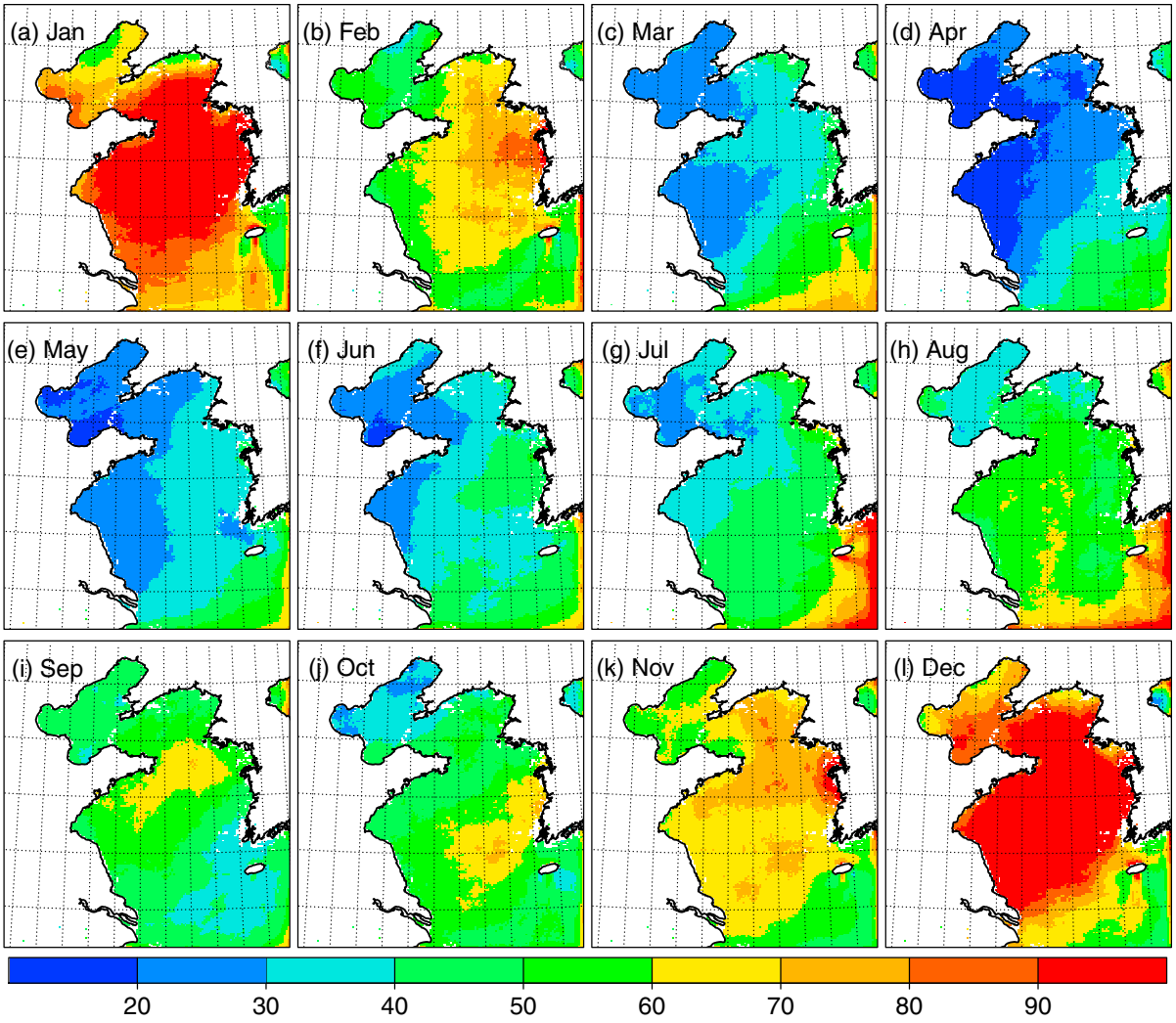

Figure 8. Spatial distributions of relative standard deviation of low-level jet monthly frequency occurrence in percentage (%).

4.2. Diagnosis of the Intra-Annual Variations of the Simulated LLJs

The simulated LLJs exhibit pronounced intra-annual variability, in particular, a clear temporal mismatch between the monthly annual cycle of LLJ frequencies and wind speeds, as shown in the last section. We selected June (with high LLJ occurrence and medium LLJ wind speed) and December (with very low LLJ occurrence frequency and medium LLJ wind speed) to determine the possible reasons.

Figures 9a and 9b show the monthly averaged fields of the mean sea level pressure (MSLP) and the wind speed at a 404-m height from ERAI reanalysis for June and December, respectively. In June, there is a high-pressure system over the northwest Pacific Ocean and a low-pressure system over the Asian continent. Winds over the BYS at a 404-m height are predominantly southerly and southeasterly. In winter, the pressure system and wind direction reverse, with a high-pressure system over the Asian continent and a low-pressure system over the Pacific Ocean; winds are generally northerly and northwesterly. The geostrophic winds due to the large-scale pressure gradient preconditions the wind intensity associated with the LLJs over the BYS, which is consistent with Du et al. (2014), who found that geostrophic winds dominate actual winds near LLJ cores off the Chinese southeastern coasts. The seasonal variation of large-scale atmospheric circulations related to East Asian monsoon is thought to greatly influence the monthly variability of LLJ wind intensity over the BYS.

However, the combination of strong low-level winds and significant vertical shear of horizontal winds defines the LLJs over the BYS. The later factor contributes to the increased jet-like structure in June compared to December.

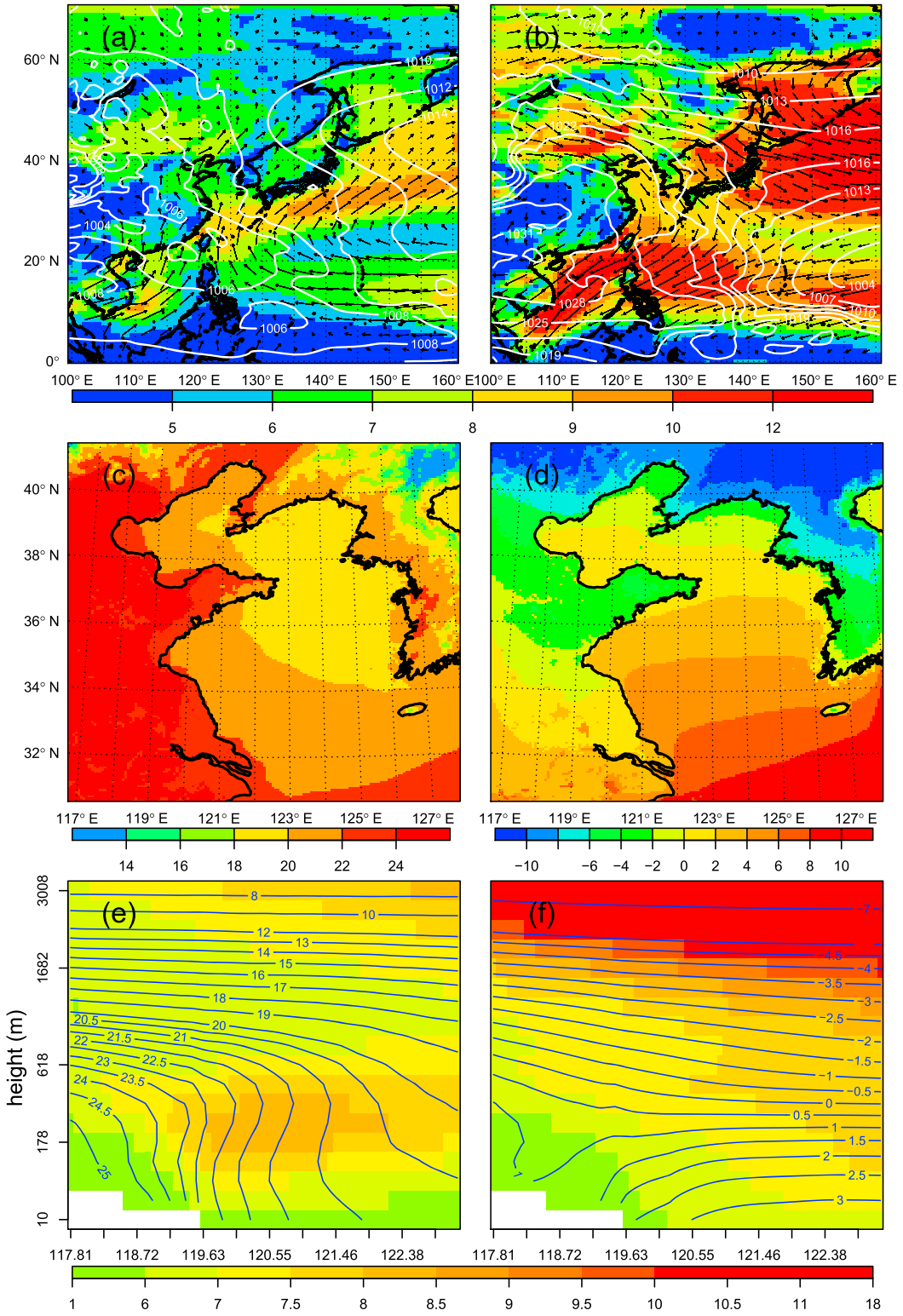

Figure 9. Monthly climatological mean (1979–2013) for (a and b) wind speed (shading), wind vector (arrows) at 404-m height and sea level pressure (white contours) of ERA-Interim reanalysis data set; (c and d) 2-m temperature (shading and red contours) of climate model COSMO-CLM data set, (e and f) wind speed (shading) and temperature (contours) of climate model COSMO-CLM data set at black cross section in Figure 1. Left panels are for June, while right panels for December.

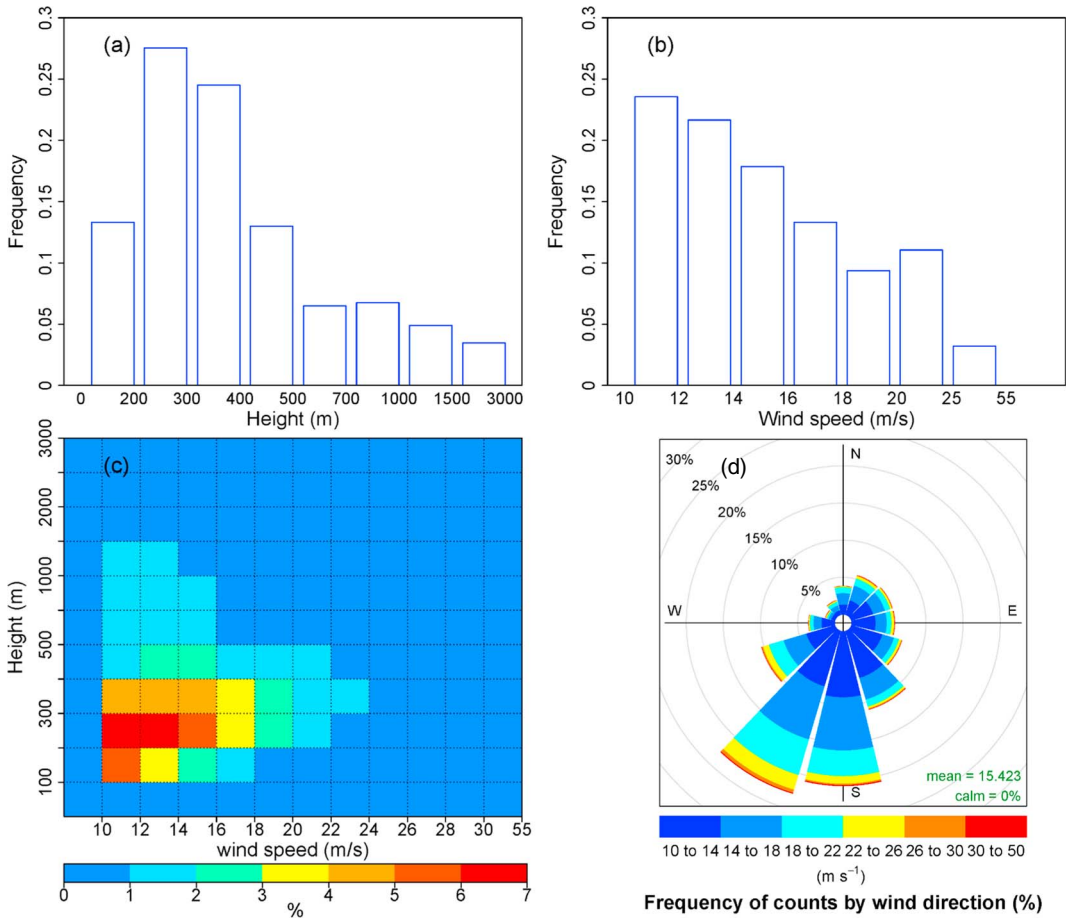

Figure 10. Low-level jets statistics over the Bohai Sea and Yellow Sea during April, May, and June (1979–2013): (a) Jet height histogram (%), (b) jet wind speed histogram (%), (c) jet height-wind speed distribution, and (d) jet wind rose.

In addition to the differences in large-scale circulation, Figures 9c and 9d show that there are great differences in the local land-sea thermal contrast between June and December over the BYS. The temperature contours are generally coastline parallel in June, while they are mainly zonal parallel in December. The presence of a pronounced zonal thermal contrast in June (Figure 9e) leads to a local thermal circulation, with easterly ageostrophic winds at low levels. This ageostrophic wind is further affected by the Coriolis force, generating southerly flow and superimposing on the large-scale southerly or southeasterly geostrophic winds (Figure 9a). Hence, an intensified local wind speed at low level is generated, with a generally coastal-parallel direction. In the upper levels, the thermal contrast is not pronounced, resulting in relatively weak wind. The friction effect is thought to reduce the intensity of bottom winds. This strong low-level thermal contrast and the friction effect contribute to more frequent LLJs in June than in December.

5. Variability and Large-Scale Conditioning During LLJ Season

LLJ activity is particularly pronounced in the LLJ season of April, May, and June, contributing from large-scale circulations and local land-sea thermal contrast, as was demonstrated in the previous section. In the following section, we will discuss in more detail the diurnal and decadal variability, as well as the link to large-scale atmospheric patterns, during this season.

5.1. Features of LLJs in the LLJ Season

LLJ statistics in the LLJ season (Figure 10) show that more than 50% of jet core heights over the BYS area are distributed in the range of 200–400 m, more than 75% are below 500 m, and 96% are below 1500 m. In terms of the wind speed of jet cores, approximately 45% are in the range of 10–14 m/s, 96.8% are below 25 m/s.

More than 3% of LLJs are characterized as having extremely strong wind speeds between 25 and 55 m/s. The jet height-wind speed distribution diagram (Figure 10c) indicates that the jet cores are mostly located between 200 and 400 m with speed in the range of 10–16 m/s. The prevailing wind directions of LLJs (Figure 10d) are southwesterly (~22.5% south-southwesterly and ~10% west-southwesterly), followed by southerly winds (more than 20%), which account for ~55% of the wind directions of LLJs; fewer than 20% of LLJs blow from the southeast, and the northwesterly LLJs are least frequent among all wind directions. The dominant directions of LLJs are coast parallel, which is a general feature of LLJs that results from the geostrophic adjustment between the pressure gradient force and Coriolis force (Soares et al., 2014).

The generation of LLJs in the daytime (Figures 11a–11d) is lower than in the night (Figures 11e–11h) with the former generally being lower than 30%. From 1700 (LST) on, the occurrence of LLJs begins to rise in the coastal areas of the north BS and west YS; at 2000 (LST), the occurrence is more than 30% over the BS and west coasts of the YS and up to 45% in some coastal areas. At 2300 (LST), LLJs are the most frequent, occurring in more than 35% and 50% of the time, respectively, over the BS and in the south BS. Over parts of the north and west YS, the frequency is generally greater than 30%, while it is mostly less than 20% in the coasts of the Korean Peninsula and southeast YS. At 0200 (LST), the occurrence of LLJs drops; however, it is still larger than 35% in most parts of the BS and part of west the YS. At 0500 (LST), the areas with frequent LLJs ($>$35%) shrink to the middle and south BS. In most parts of the YS, the value is less than 30%.

Furthermore, the daily cycle of occurrence frequency of jet height, jet wind speed, and wind direction over the BYS areas (Figure 12) feature by strong diurnal variability, with more LLJs from 2000 (LST) in the night to 0500 (LST) in the early morning at heights between 200 and 400 m (Figure 12a). More LLJs feature wind speeds of 10–16 m/s in the night as well (Figure 12b), and the dominant LLJ directions are southerly and south-southwesterly (Figure 12c).

Additionally, the spatial distributions of jet occurrence frequency, mean wind speed, and mean height in the LLJ seasons of 1980s, 1990s, and 2000s were obtained (see Figure S3). The results reveal generally similar spatial patterns, with some differences in the intensities for each variable among each decade. Overall, the decadal variability of LLJ features is not pronounced.

5.2. Relationship Between LLJ Occurrence and Sea Level Pressure Patterns

A critical driver of regional climate variability is the variation of large-scale atmospheric circulation (von Storch et al., 1993), which is also applicable for regional LLJ variability. Emeis (2014) found that the occurrence of LLJs over northern Germany is correlated with the appearance of typical large-scale circulation patterns. In the present study, we found that the large-scale circulation preconditions the formation of LLJs over the BYS. Here we further investigated how the large-scale circulation distributions, averaged over the LLJ season, are related to LLJ occurrence over the BYS. The MSLP from the ERAI reanalysis data set was used, covering the northwest Pacific Ocean and East Asia (0–70°N, 100°E–160°E). Notably, we did not link the instantaneous sea level pressure field with the occurrence probability of a LLJ. Instead, we related two long-term statistics, namely, the statistic of the seasonally averaged MSLP field and the seasonal LLJ occurrence frequency.

The canonical correlation analysis (CCA) method (cf. von Storch & Zwiers, 1999) was used to study the correlation structure of a pair of random vectors $\vec{X}$ and $\vec{Y}$, that is, seasonally averaged MSLP field and seasonal LLJ occurrence frequency in the present study. The objective was to identify a pair of patterns $\vec{f}^{1}_{X}$ and $\vec{f}^{1}_{Y}$ such that the time coefficients α_{1X} and α_{1Y} in optimal approximations $\vec{X} \approx \alpha_{1X}\,\vec{f}^{1}_{X}$ and $\vec{Y} \approx \alpha_{1Y}\,\vec{f}^{1}_{Y}$ share a maximum correlation. The identification of a second pair of patterns follows the same protocol. The patterns $\vec{f}^{1}_{X}$ and $\vec{f}^{1}_{Y}$ are called the canonical correlation patterns.

Before CCA analysis, we first projected the two multidimensional sets of variables onto their EOFs to exclude noise and reduce the spatial degrees of freedom. The temporal anomalies of each multidimensional data set were used in the EOF analysis. The first five EOFs of LLJ-season-mean MSLP (explaining 84.2% of the total variance) and LLJ frequency (explaining 82.6% of the total variance) were retained for the CCA analysis.

Figure 13 shows the first two important combinations of canonical patterns of LLJ-season-mean MSLP (Figures 13a and 13c) and LLJ occurrence frequency anomalies (Figures 13b and 13d) and their coefficient

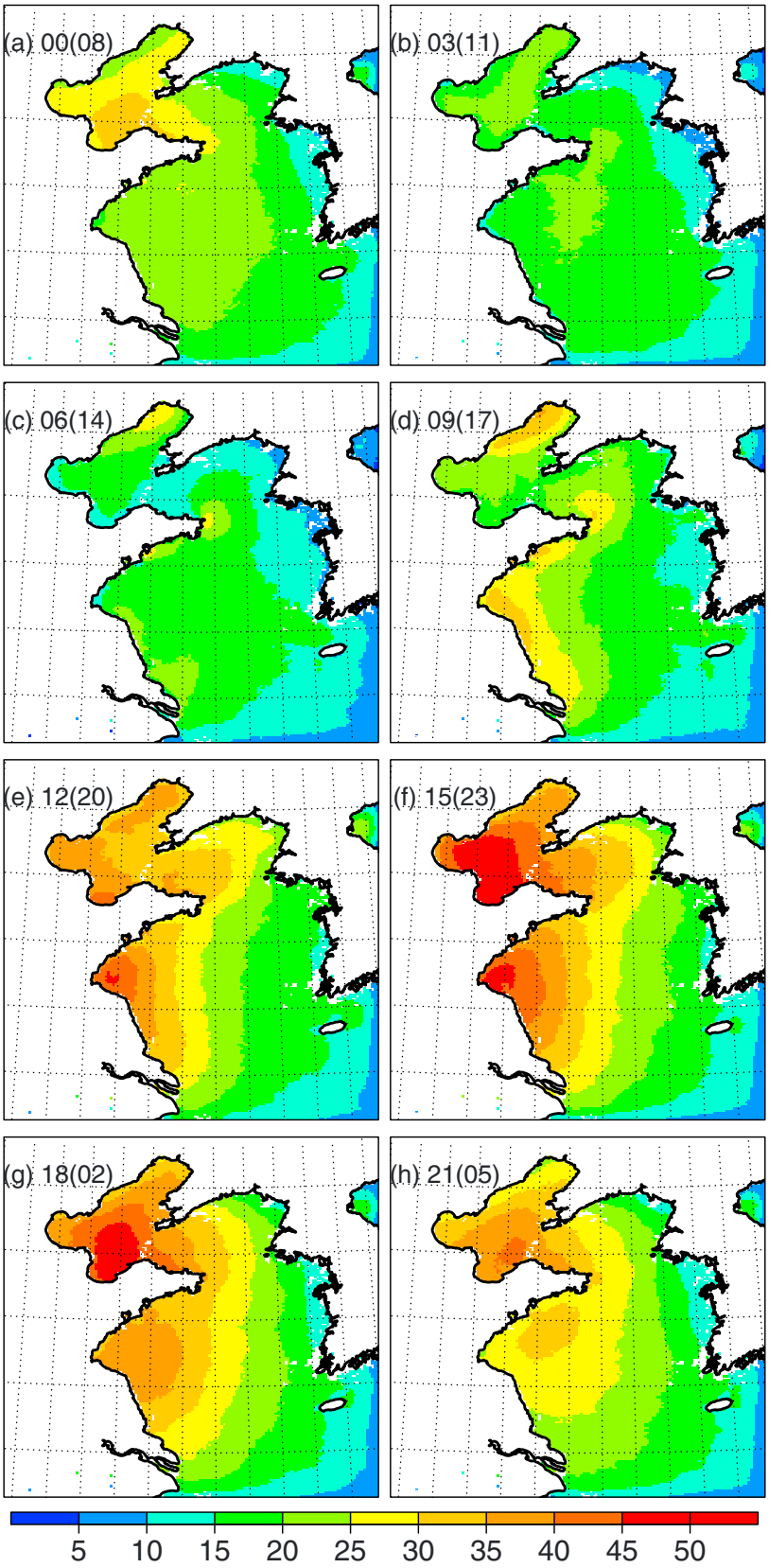

Figure 11. Diurnal variation of occurrence frequency (%) of low-level jet at a particular hour (UTC [LST]) in low-level jet season (1979–2013): (a–h) 00 (08), 03 (11), 06 (14), 09 (17), 12 (20), 15 (23), 18 (02), and 21 (05). UTC and LST are abbreviations of coordinated universal time and local solar time, respectively.

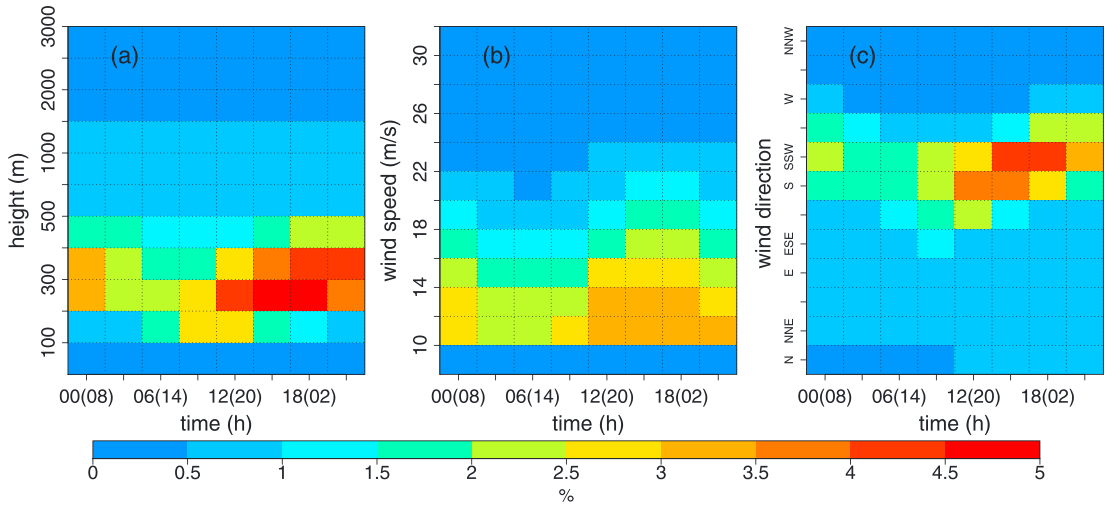

Figure 12. Diurnal cycle of low-level jet occurrence frequency in low-level jet season (1979–2013) for (a) jet height, (b) jet wind speed, and (c) jet wind direction.

time series (Figures 13e and 13f). Their coefficient time series share a correlation of 0.74 and 0.65 for CCA1 and CCA2, respectively.

The first CCA pattern of LLJ-season-mean MSLP (Figure 13a) shows a dipolar pressure distribution, indicating reversed anomalies of the subtropical high over the northwest Pacific Ocean and the northeast cold vortex over East Asia (a cyclonic circulation with a cold core at 35°N–60°N, 115°E–145°E). The first canonical pattern of LLJ occurrence frequency highly resembles the pattern of LLJs in Figures 7d–7f over the northern and western region of the BYS. When the coefficient is positive, a northeastward geostrophic flow anomaly is present, which is consistent with the dominant direction of LLJs, preconditioning more frequent LLJs over the northern and western region of BYS. A pressure contrast of approximately 1.5 hPa between the northwest Pacific Ocean and northeast Asia is related to 0.6% to 2.4% more LLJs in the most BYS region. When the coefficient is negative, the patterns of LLJ-season-mean MSLP and LLJs reverse. The coefficient time series (Figure 13e) reflect that CCA1 dominated in 1998 with more LLJ, and in 1979, 1984, 1992, and 1996 with fewer LLJs, in the northern and western regions of the BYS.

Another covariability is described by the second canonical pattern (Figures 13c and 13d). In the case of CCA2 of MSLP, there is a negative anomaly over the Sea of Okhotsk and two positive anomalies over East Asia and east to Japan. In the case of positive coefficients, the contrast between the pressure over East Asia and east to Japan, as well as the Sea of Okhotsk, induces southward or southwestward geostrophic flow anomalies, which result in fewer LLJs in the eastern and southern parts of the BYS. Based on the coefficient time series (Figure 13f), CCA2 dominated in the years 1991, 1998, and 2003, with fewer LLJs, and in the years 2005 and 2006, with more LLJs over the southern and eastern parts of the BYS region.

5.3. Relationship Between LLJ Occurrence and Upper-Level Atmospheric Circulations

To reveal the relationship between LLJ occurrence frequency and upper-level atmospheric circulations, the associated correlation pattern (ACP) approach (von Storch & Zwiers, 1999) was used in this study. ACP is a method based on a linear statistical model, which relates an index of some process with a physical field. We used the coefficient time series for the first two CCA patterns of LLJ occurrence frequency as indices to derive their relationship with geopotential heights at different pressure levels, that is, at 200, 500, and 950 hPa, in the LLJ season by means of linear correlation coefficients.

The ACP patterns at different heights (Figure 14) are rather similar among each other and to the corresponding CCA of MSLP field (Figures 13a and 13c), with the patterns becoming weaker with height. In the case of CCA1 (Figure 14, left panel), negative correlations prevail over northeast Asia and positive values over the northwest Pacific Ocean. In the case of CCA2 (Figure 14, right panel), there are negative values over the Sea of Okhotsk and positive values over East China and the northwest Pacific Ocean. These results indicate that the link between regional large-scale circulations and LLJ occurrence frequency is generally

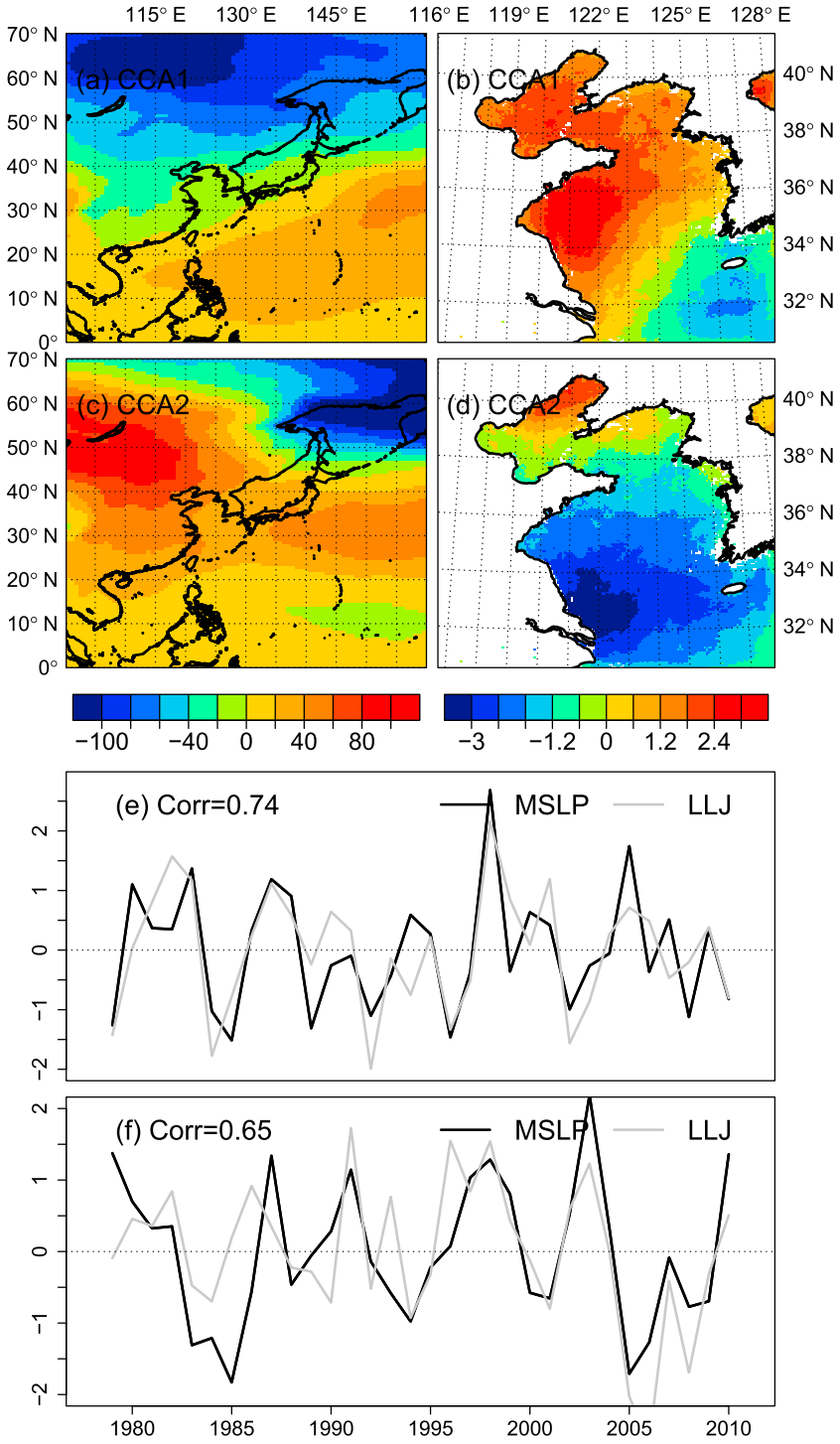

Figure 13. First two canonical correlation patterns of MSLP (a and c, unit Pa) and LLJ (c and d, unit: %). Corresponding coefficient time series (e and f) for the first two canonical correlation analysis (CCA) patterns, respectively. The first CCA pair shares a correlation of 0.74 and second CCA pair share a correlation of 0.65. MSLP = mean sea level pressure; LLJ = low-level jet; CCA = canonical correlation analysis.

barotropic, with similar patterns from top to bottom. The atmospheric circulation in the bottom level has a stronger relationship with LLJ occurrence frequency than that in the upper levels.

The change of the mean state of the barotropic circulation and the associated geostrophic flow is indicative for a synoptic situation, which favor or disfavor the formation of LLJs. Indeed, we consider LLJs as short-term

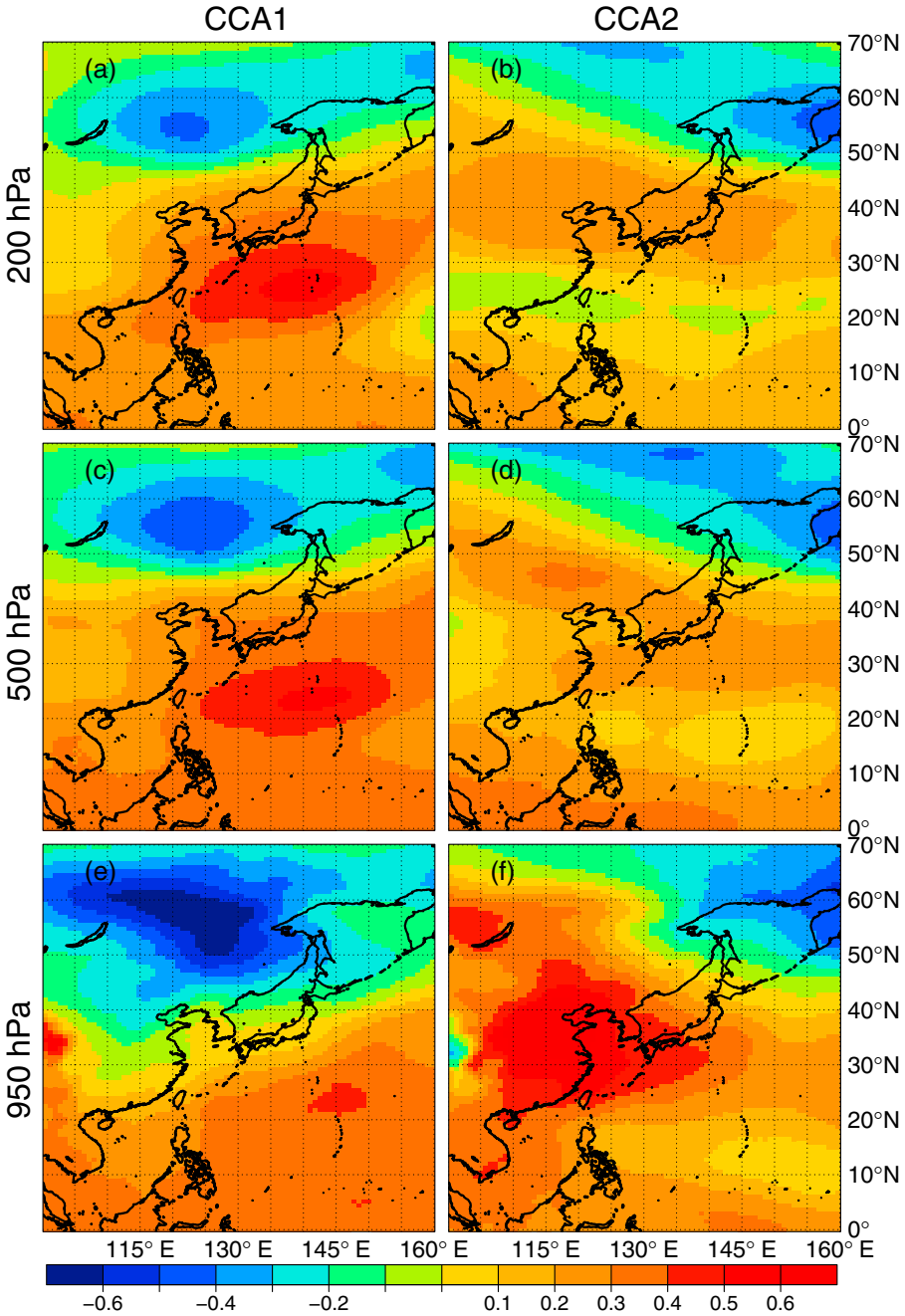

Figure 14. Associated correlation patterns between geopotential height anomalies (from top to bottom 200, 500, and 950 hPa) and coefficient time series for the first two canonical correlation analysis (CCA) patterns of low-level jet occurrence frequency (left panel: CCA1, right panel: CCA2).

random events (von Storch et al., 2001; similar to Polar Lows and their formation in cold air outbreaks: Kolstad et al., 2009) and not as deterministic features—with probabilities conditioned by the regional synoptic situation, which is well described by the barotropic and geostrophic state. The physical processes that are instrumental in actual formation of a LLJ may well not be barotropic nor geostrophic, but their presence seems to be strongly linked to changes in the low-frequency regional barotropic and geostrophic state. Since the statistics of the latter vary more slowly, we are able to construct a link of the circulation over the

Asian continent and the northwest Pacific Ocean and the tendency of forming or nonforming LLJs in the coastal regions of BYS.

6. Summary and Conclusions

In the present study, the climatology and variability features of LLJs over the BYS were investigated based on a long-term (1979–2013) high-resolution (7 km) atmospheric hindcast, which was produced by a regional climate model (CCLM) constrained by ERA-Interim reanalysis. The high-resolution data set was of good quality in terms of its ability to reproduce surface wind speeds and coastal mesoscale phenomena in comparison with observations (Li, 2017; Li, von Storch, & Geyer, 2016a). In this study, we further verified the data set against several radiosonde observations and wind profiler radar observations. The CCLM data set was found to robustly capture the climatology of wind profiles, daily cycle feature, and variability of wind speeds, as well as LLJ cases.

Following the selection criteria by Bonner (1968), the occurrence, height, strength, and direction of LLJs over the BYS spanning 1979–2013 were identified. The annual occurrence of LLJs is more frequent in the BS and western part of the YS. In terms of the temporal variability of LLJs on different scales, we found that the LLJs are nocturnal type LLJs, with the highest occurrence frequency at approximately 2300 (LST). LLJs are the most frequent from April to June, with their occurrence generally exceeding 21% for much of the BYS. The frequency can be greater than 30% over the BS and part of western YS. LLJs are the least frequent in winter, with an occurrence frequency generally less than 12%. The intra-annual variations of LLJ features were found to be related to large-scale circulation and local land-sea thermal contrast. The friction effect is also important in the formation of LLJs over the BYS.

The relative interannual variability of the monthly frequency is generally greater than 20% in most areas. Strong interannual variability exists for LLJs over the BYS, especially during months when the LLJ occurrence is less frequent. In LLJ season (April, May, and June), the heights of jet cores are mostly between 200 and 400 m above sea level, with wind speed maxima mostly in the range of 10–16 m/s. The prevailing wind directions are southerly and southwesterly, which account for approximately 55% of all LLJ directions. Furthermore, we did not find strong interdecadal variability of LLJ features over the BYS in recent decades.

Furthermore, it is thought that the mean state of large-scale atmospheric barotropic circulations over the Asian continent and the northwest Pacific Ocean favors synoptic situations, which precondition LLJ occurrence over the BYS. A link between LLJ occurrence frequency and regional large-scale barotropic circulations has been shown in terms of the low-frequency variability on the interannual scale.

This is the first study to document the long-term climatology and variability of LLJs in Chinese water areas using a high-resolution model output. However, several issues should be addressed. First, the LLJ detection was based on a 3-hr vertical output because of the initial model setup. A higher-frequency temporal output, that is, 1 hr, may enable a more detailed description of the climatological features of LLJs over the BYS, especially for diurnal variability. Second, the detection method defines basic LLJs of jet-like wind profile, while advanced detection method (e.g., Lima et al., 2018) is suggested to apply in defining typical coastal LLJs (e.g., Ranjha et al., 2013) with specific generation mechanism and jet features. Third, we only investigated the link between LLJs and regional atmospheric circulations in terms of low-frequency variability; however, the influences of local baroclinicity or other mesoscale processes on LLJ features, as well as the extension of the contribution of large-scale processes versus local/mesoscale processes to LLJs in terms of long-term variability, have not been studied, and they deserve further study in the future. Finally, issues such as the impacts of LLJs on regional weather (extreme rainfall), ocean dynamics (circulation and upwelling), and human applications, such as offshore wind farms, have not been studied in the East China Sea and deserve further in-depth study.

Acknowledgments

We thank Beate Geyer and Burkhardt Rockel for their help in the regional climate modeling and statistical processing. Thanks to the two reviewers (Pedro M. M. Soares and another anonymous reviewer) for their constructive comments and helpful suggestions. We thank the German Climate Computing Center (DKRZ) for providing the computer hardware for our simulation (available at https://cera-www.dkrz.de/WDCC/ui/cerasearch/entry?acronym=BH_LONG_ERAin). The publicly accessible data sets used in the study are greatly appreciated: the reanalysis data set ERA-Interim obtained from the European Centre for Medium-Range Weather Forecasts (ECMWF, http://apps.ecmwf.int/datasets/data/interim-full-daily) following registration, the model external forcing data obtained freely from the Climate Limited-area Modeling-Community (http://www.clm-community.eu/index.php?menuid=221), and sounding observations obtained from the University of Wyoming (http://weather.uwyo.edu/upperair/sounding.html) by contacting Larry Oolman. Funding for this study was provided by the Qingdao National Laboratory for Marine Science and Technology (2016ASKJ12), the National Key Research and Development Program of China (2017YFA0604100 and 2016YFC1401404), the National Natural Science Foundation of China (41706019, 41528601, 41676006, U1606402, and 41421005), the General Financial Grant (2017M612357), and Special Financial Grant (2017T100520) from the China Postdoctoral Science Foundation, Youth Innovation Promotion Association Chinese Academy of Sciences (CAS), CAS Interdisciplinary Innovation Team, Key Research Program of Frontier Sciences, CAS, and the Strategic Pioneering Research Program of CAS (XDA11020104 and XDA11020101).

References

Arfeuille, G., Quintanilla-Montoya, A. L., Viesca González, F. C., & Zizumbo Villarreal, L. (2015). Observational characteristics of low-level jets in central western Mexico. *Boundary-Layer Meteorology*, *6*, 483–500.

Beardsley, R. C., Dorman, C. E., Friehe, C. A., Rosenfeld, L. K., & Winant, C. D. (1987). Local atmospheric forcing during the Coastal Ocean Dynamics Experiment: 1. A description of the marine boundary layer and atmospheric conditions over a northern California upwelling region. *Journal of Geophysical Research*, *92*, 1467–1488. https://doi.org/10.1029/JC092iC02p01467

Blackadar, A. K. (1957). Boundary layer wind maxima and their significance for the growth of nocturnal inversions. *Bulletin of the American Meteorological Society*, *38*, 283–290.

Bonner, W. D. (1968). Climatology of the low level jet. *Monthly Weather Review*, *96*(12), 833–885.
Burk, S. D., & Thompson, W. T. (1996). The summertime low-level jet and marine boundary layer structure along the California coast. *Monthly Weather Review*, *124*(4), 668–686. https://doi.org/10.1175/1520-0493(1996)124%3C0668:TSLLJA%3E2.0.CO;2
Cardoso, R. M., Soares, P. M., Lima, D. C., & Semedo, A. (2016). The impact of climate change on the Iberian low-level wind jet: EURO-CORDEX regional climate simulation. *Tellus A: Dynamic Meteorology and Oceanography*, *68*(1), 29005. https://doi.org/10.3402/tellusa.v68.29005
Chao, S.-Y. (1985). Coastal jets in the lower atmosphere. *Journal of Physical Oceanography*, *15*(4), 361–371. https://doi.org/10.1175/1520-0485(1985)015%3C0361:CJITLA%3E2.0.CO;2
Chen, G. T.-J., Wang, C.-C., & Lin, D. T.-W. (2005). Characteristics of low-level jets over northern Taiwan in Mei-Yu season and their relationship to heavy rain events. *Monthly Weather Review*, *133*(1), 20–43. https://doi.org/10.1175/MWR-2813.1
Colle, B. A., & Novak, D. R. (2010). The New York bight jet: Climatology and dynamical evolution. *Monthly Weather Review*, *138*(6), 2385–2404. https://doi.org/10.1175/2009MWR3231.1
Cook, K. H., & Vizy, E. K. (2010). Hydrodynamics of the Caribbean low-level jet and its relationship to precipitation. *Journal of Climate*, *23*(6), 1477–1494. https://doi.org/10.1175/2009JCLI3210.1
Dee, D. P., & National Center for Atmospheric Research Staff (2018). The climate data guide: ERA-Interim. Retrieved from https://climate-dataguide.ucar.edu/climate-data/era-interim, Accessed 15 March 2018.
Dee, D. P., Uppala, S. M., Simmons, A. J., Berrisford, P., Poli, P., Kobayashi, S., et al. (2011). The ERA-Interim reanalysis: Configuration and performance of the data assimilation system. *Quarterly Journal of the Royal Meteorological Society*, *137*(656), 553–597. https://doi.org/10.1002/qj.828
Doubler, D. L., Winkler, J. A., Bian, X., Walters, C. K., & Zhong, S. (2015). An NARR-derived climatology of southerly and northerly low-level jets over North America and coastal environs. *Journal of Applied Meteorology and Climatology*, *54*(7), 1596–1619. https://doi.org/10.1175/JAMC-D-14-0311.1
Doyle, J. D., & Warner, T. T. (1993). A three-dimensional numerical investigation of a Carolina coastal low-level jet during GALE IOP 2. *Monthly Weather Review*, *121*(4), 1030–1047. https://doi.org/10.1175/1520-0493(1993)121%3C1030:ATDNIO%3E2.0.CO;2
Du, Y., Chen, Y.-L., & Zhang, Q. (2015). Numerical simulations of the boundary layer jet off the southeastern coast of China. *Monthly Weather Review*, *143*(4), 1212–1231. https://doi.org/10.1175/MWR-D-14-00348.1
Du, Y., Zhang, Q., Chen, Y., Zhao, Y., & Wang, X. (2014). Numerical simulations of spatial distributions and diurnal variations of low-level jets in China during early summer. *Journal of Climate*, *27*(15), 5747–5767. https://doi.org/10.1175/JCLI-D-13-00571.1
Emeis, S. (2014). Wind speed and shear associated with low-level jets over Northern Germany. *Meteorologische Zeitschrift*, *23*(3), 295–304. https://doi.org/10.1127/0941-2948/2014/0551
Higgins, R. W., Yao, Y., Yarosh, E. S., Janowiak, J. E., & Mo, K. C. (1997). Influence of the Great Plains low-level jet on summertime precipitation and moisture transport over the Central United States. *Journal of Climate*, *10*(3), 481–507. https://doi.org/10.1175/1520-0442(1997)010%3C0481:IOTGPL%3E2.0.CO;2
Jiang, Q., Wang, S., & O'Neill, L. (2010). Some insights into the characteristics and dynamics of the Chilean low-level coastal jet. *Monthly Weather Review*, *138*(8), 3185–3206. https://doi.org/10.1175/2010MWR3368.1
Kolstad, E., Bracegirdle, T. J., & Seierstad, I. A. (2009). Marine cold-air outbreaks in the North Atlantic: Temporal distribution and associations with large-scale atmospheric circulation. *Climate Dynamics*, *33*, 187–197. https://doi.org/10.1007/s00382-008-0431-5
Li, D., Geyer, B., & Bisling, P. (2016). A model-based climatology analysis of wind power resources at 100-m height over the Bohai Sea and the Yellow Sea. *Applied Energy*, *179*, 575–589. https://doi.org/10.1016/j.apenergy.2016.07.010
Li, D., von Storch, H., & Geyer, B. (2016a). High-resolution wind hindcast over the Bohai Sea and the Yellow Sea in East Asia: Evaluation and wind climatology analysis. *Journal of Geophysical Research: Atmospheres*, *121*, 111–129. https://doi.org/10.1002/2015JD024177
Li, D., von Storch, H., & Geyer, B. (2016b). Testing reanalyses in constraining dynamical downscaling. *Journal of the Meteorological Society of Japan Series II*, *94A*, 47–68. https://doi.org/10.2151/jmsj.2015-044
Li, D. L. (2017). Added value of high-resolution regional climate model: Selected cases over the Bohai Sea and the Yellow Sea areas. *International Journal of Climatology*, *37*(1), 169–179. https://doi.org/10.1002/joc.4695
Lima, D. C. A., Soares, P. M. M., Semedo, A., & Cardoso, R. M. (2018). A global view of coastal low-level wind jets using an ensemble of reanalyses. *Journal of Climate*, *31*(4), 1525–1546. https://doi.org/10.1175/JCLI-D-17-0395.1
Maddox, R. A. (1983). Large-scale meteorological conditions associated with midlatitude, mesoscale convective complexes. *Monthly Weather Review*, *111*(7), 1475–1493. https://doi.org/10.1175/1520-0493(1983)111%3C1475:LSMCAW%3E2.0.CO;2
Maldonado, T., Rutgersson, A., Caballero, R., Pausata, F. S. R., Alfaro, E., & Amador, J. (2017). The role of the meridional sea surface temperature gradient in controlling the Caribbean low-level jet: Meridional SST gradient and CLLJ. *Journal of Geophysical Research: Atmospheres*, *122*, 5903–5916. https://doi.org/10.1002/2016JD026025
Marengo, J. A., Soares, W. R., Saulo, C., & Nicolini, M. (2004). Climatology of the low level jet east of the Andes as derived from the NCEP-NCAR reanalyses: Characteristics and temporal variability. *Journal of Climate*, *17*(12), 2261–2280. https://doi.org/10.1175/1520-0442(2004)017%3C2261:COTLJE%3E2.0.CO;2
Means, L. Y. N. N. L. (1954). A study of the mean southerly wind maximum in low levels associated with a period of summer precipitation in the middle west. *Bulletin of the American Meteorological Society*, *35*, 166–170.
Mellor, G. L., & Yamada, T. (1982). Development of a turbulence closure model for geophysical fluid problems. *Reviews of Geophysics*, *20*, 851–875. https://doi.org/10.1029/RG020i004p00851
Miao, Y., Guo, J., Liu, S., Wei, W., Zhang, G., Lin, Y., & Zhai, P. (2018). The climatology of low-level jet in Beijing and Guangzhou, China. *Journal of Geophysical Research: Atmospheres*, *123*, 2816–2830. https://doi.org/10.1002/2017JD027321
Muñoz, E., & Enfield, D. (2011). The boreal spring variability of the Intra-Americas low-level jet and its relation with precipitation and tornadoes in the eastern United States. *Climate Dynamics*, *36*(1–2), 247–259. https://doi.org/10.1007/s00382-009-0688-3
Nicholson, S. E. (2010). A low-level jet along the Benguela coast, an integral part of the Benguela current ecosystem. *Climatic Change*, *99*(3–4), 613–624. https://doi.org/10.1007/s10584-009-9678-z
Nunalee, C. G., & Basu, S. (2013). Mesoscale modeling of coastal low-level jets: Implications for offshore wind resource estimation. *Wind Energy*, *17*(8), 1199–1216.
Nuss, W. A., Bane, J. M., Thompson, W. T., Holt, T., Dorman, C. E., Ralph, F. M., et al. (2000). Coastally trapped wind reversals: Progress toward understanding. *Bulletin of the American Meteorological Society*, *81*(4), 719–743. https://doi.org/10.1175/1520-0477(2000)081%3C0719:CTWRPT%3E2.3.CO;2
Parish, T. R. (2000). Forcing of the summertime low-level jet along the California coast. *Journal of Applied Meteorology*, *39*(12), 2421–2433. https://doi.org/10.1175/1520-0450(2000)039%3C2421:FOTSLL%3E2.0.CO;2

Parish, T. R., & Oolman, L. D. (2010). On the role of sloping terrain in the forcing of the Great Plains low-level jet. *Journal of the Atmospheric Sciences*, *67*(8), 2690–2699. https://doi.org/10.1175/2010JAS3368.1

Pham, N., Nakamura, K., Furuzawa, F. A., & Satoh, S. (2008). Characteristics of low level jets over Okinawa in the Baiu and post-Baiu seasons revealed by wind profiler observations. *Journal of the Meteorological Society of Japan*, *86*(5), 699–717. https://doi.org/10.2151/jmsj.86.699

Rahn, D. A., & Parish, T. R. (2007). Diagnosis of the forcing and structure of the coastal jet near Cape Mendocino using in situ observations and numerical simulations. *Journal of Applied Meteorology and Climatology*, *46*(9), 1455–1468. https://doi.org/10.1175/JAM2546.1

Ranjha, R., Svensson, G., Tjernström, M., & Semedo, A. (2013). Global distribution and seasonal variability of coastal low-level jets derived from ERA-Interim reanalysis. *Tellus A*, 65.

Ranjha, R., Tjernström, M., Semedo, A., Svensson, G., & Cardoso, R. M. (2015). Structure and variability of the Oman coastal low-level jet. *Tellus A*, *67*(1), 25285. https://doi.org/10.3402/tellusa.v67.25285

Ranjha, R., Tjernström, M., Svensson, G., & Semedo, A. (2016). Modelling coastal low-level wind-jets: does horizontal resolution matter? *Meteorology and Atmospheric Physics*, *128*(2), 263–278.

Rijo, N., Semedo, A., Miranda, P. M. A., Lima, D., Cardoso, R. M., & Soares, P. M. M. (2018). Spatial and temporal variability of the Iberian Peninsula coastal low-level jet. *International Journal of Climatology*, *38*(4), 1605–1622. https://doi.org/10.1002/joc.5303

Rockel, B., Will, A., & Hense, A. (2008). The regional Climate Model COSMO-CLM (CCLM). *Meteorologische Zeitschrift*, *17*(4), 347–348. https://doi.org/10.1127/0941-2948/2008/0309

Schrodin, R., & Heise, E. (2002). A new multi-layer soil model. *COSMO Newsletter*, *2*, 149–151.

Semedo, A., Soares, P. M. M., Lima, D. C. A., Cardoso, R. M., Bernardino, M., & Miranda, P. M. A. (2016). The impact of climate change on the global coastal low-level wind jets: EC-EARTH simulations. *Global and Planetary Change*, *137*, 88–106. https://doi.org/10.1016/j.gloplacha.2015.12.012

Soares, P. M. M., Cardoso, R. M., Semedo, A., Chinita, M. J., & Ranjha, R. (2014). Climatology of the Iberia coastal low-level wind jet: Weather research forecasting model high-resolution results. *Tellus A*, *66*(1), 22377. https://doi.org/10.3402/tellusa.v66.22377

Soares, P. M. M., Lima, D. C. A., Cardoso, R. M., & Semedo, A. (2017). High resolution projections for the western Iberian coastal low level jet in a changing climate. *Climate Dynamics*, *49*(5–6), 1547–1566. https://doi.org/10.1007/s00382-016-3397-8

Stensrud, D. J. (1996). Importance of low-level jets to climate: A review. *Journal of Climate*, *9*(8), 1698–1711. https://doi.org/10.1175/1520-0442(1996)009%3C1698:IOLLJT%3E2.0.CO;2

Tao, S. Y., & Chen, L. A. (1987). A review of recent research on the East Asian summer monsoon in China. In *Monsoon meteorology* (pp. 60–92). Oxford, UK: Oxford University Press.

Tiedtke, M. (1989). A comprehensive mass flux scheme for cumulus parameterization in large-scale models. *Monthly Weather Review*, *117*(8), 1779–1800. https://doi.org/10.1175/1520-0493(1989)117%3C1779:ACMFSF%3E2.0.CO;2

von Storch, H., Langenberg, H., & Feser, F. (2000). A spectral nudging technique for dynamical downscaling purposes. *Monthly Weather Review*, *128*(10), 3664–3673. https://doi.org/10.1175/1520-0493(2000)128%3C3664:ASNTFD%3E2.0.CO;2

von Storch, H., von Storch, J.-S., & Müller, P. (2001). Noise in the climate system—Ubiquitous, constitutive and concealing. In B. Engquist, & W. Schmid (Eds.), *Mathematics unlimited—2001 and beyond. Part II* (pp. 1179–1194). Berlin, DE: Springer Verlag. https://doi.org/10.1007/978-3-642-56478-9_62

von Storch, H., Zorita, E., & Cubasch, U. (1993). Downscaling of global climate change estimates to regional scales: An application to Iberian rainfall in wintertime. *Journal of Climate*, *6*(6), 1161–1171. https://doi.org/10.1175/1520-0442(1993)006%3C1161:DOGCCE%3E2.0.CO;2

von Storch, H., & Zwiers, F. W. (1999). *Statistical analysis in climate research*. Cambridge, UK: Cambridge University Press. https://doi.org/10.1017/CBO9780511612336

Wang, D., Zhang, Y., & Huang, A. (2013). Climatic features of the south-westerly low-level jet over Southeast China and its association with precipitation over East China. *Asia-Pacific Journal of Atmospheric Sciences*, *49*(3), 259–270. https://doi.org/10.1007/s13143-013-0025-y

Warner, T. T. (2004). *Desert meteorology*. Cambridge, UK: Cambridge University Press. https://doi.org/10.1017/CBO9780511535789

Wei, W., Wu, B. G., Ye, X. X., Wang, H. X., & Zhang, H. S. (2013). Characteristics and mechanisms of low-level jets in the Yangtze River Delta of China. *Boundary-Layer Meteorology*, *149*(3), 403–424. https://doi.org/10.1007/s10546-013-9852-8

Wei, W., Zhang, H. S., & Ye, X. X. (2014). Comparison of low-level jets along the north coast of China in summer. *Journal of Geophysical Research: Atmospheres*, *119*(16), 9692–9706. https://doi.org/10.1002/2014JD021476

Whiteman, C. D., Bian, X., & Zhong, S. (1997). Low-level jet climatology from enhanced Rawinsonde observations at a site in the southern Great Plains. *Journal of Applied Meteorology*, *36*(10), 1363–1376. https://doi.org/10.1175/1520-0450(1997)036%3C1363:LLJCFE%3E2.0.CO;2

Whyte, F. S., Taylor, M. A., Stephenson, T. S., & Campbell, J. D. (2007). Features of the Caribbean low level jet. *International Journal of Climatology*, *28*(1), 119–128. https://doi.org/10.1002/joc.1510

Winant, C. D., Dorman, C. E., Friehe, C. A., & Beardsley, R. C. (1988). The marine layer off northern California: An example of supercritical channel flow. *Journal of the Atmospheric Sciences*, *45*(23), 3588–3605. https://doi.org/10.1175/1520-0469(1988)045%3C3588:TMLONC%3E2.0.CO;2

Wu, Y., & Raman, S. (1998). The summertime Great Plains low level jet and the effect of its origin on moisture transport. *Boundary-Layer Meteorology*, *88*(3), 445–466. https://doi.org/10.1023/A:1001518302649